

Geology

Dynamic rupture experiments elucidate tensile crack development during propagating earthquake ruptures

W. Ashley Griffith, Ares Rosakis, David D. Pollard and Chi Wan Ko

Geology 2009;37:795-798

doi: 10.1130/G30064A.1

Email alerting services

click www.gsapubs.org/cgi/alerts to receive free e-mail alerts when new articles cite this article

Subscribe

click www.gsapubs.org/subscriptions/ to subscribe to *Geology*

Permission request

click <http://www.geosociety.org/pubs/copyrt.htm#gsa> to contact GSA

Copyright not claimed on content prepared wholly by U.S. government employees within scope of their employment. Individual scientists are hereby granted permission, without fees or further requests to GSA, to use a single figure, a single table, and/or a brief paragraph of text in subsequent works and to make unlimited copies of items in GSA's journals for noncommercial use in classrooms to further education and science. This file may not be posted to any Web site, but authors may post the abstracts only of their articles on their own or their organization's Web site providing the posting includes a reference to the article's full citation. GSA provides this and other forums for the presentation of diverse opinions and positions by scientists worldwide, regardless of their race, citizenship, gender, religion, or political viewpoint. Opinions presented in this publication do not reflect official positions of the Society.

Notes

Dynamic rupture experiments elucidate tensile crack development during propagating earthquake ruptures

W. Ashley Griffith^{1*}, Ares Rosakis², David D. Pollard¹, and Chi Wan Ko²

¹Department of Geological and Environmental Sciences, Stanford University, Stanford, California 94305, USA

²Graduate Aeronautical Laboratories, California Institute of Technology, Pasadena, California 91125, USA

ABSTRACT

We used optical experiments and high-speed photography to interpret the origins of tensile fractures that form during dynamic shear rupture in laboratory experiments. Sub-Rayleigh (slower than the Rayleigh wave speed, c_R) shear ruptures in Homalite-100 produce damage zones consisting of an array of tensile cracks. These cracks nucleate and grow within cohesive zones behind the tips of shear ruptures that propagate dynamically along interfaces with frictional and cohesive strength, simulating a “strong” fault. The tensile cracks are produced only along one side of the interface where transient, fault-parallel, tensile stress perturbations are associated with the growing shear rupture tip. Results of this study represent an important potential bridge between geological observations of structures preserved along exhumed faults and theoretical models of earthquake propagation, potentially leading to diagnostic criteria for interpreting velocity, directivity, and static prestress states associated with past earthquakes on exhumed faults.

INTRODUCTION

Direct observation of ancient faults exhumed from hypocentral depths can provide high-precision data related to the local boundary conditions controlling earthquake rupture propagation (Chester et al., 1993; Wibberley and Shimamoto, 2003; Di Toro et al., 2005a, 2005b; Griffith et al., 2008). However, field-based studies of faults typically address fault development as a quasi-static problem occurring on time scales of 1 ka to 1 Ma and greater (Willemsse and Pollard, 1998; Mutlu and Pollard, 2008). Direct evidence of processes operating on shorter time scales during faulting is generally erased from rocks due to overprinting events, chemical changes, and structural alterations. Differentiation between faults that hosted earthquakes and those that slipped aseismically is nearly impossible, save for the rare occurrence of pseudotachylyte, a rock that is formed by melting associated with frictional heating during earthquakes (Cowan, 1999). Other structural features in rocks that may be indicative of dynamic (earthquake) processes are indistinguishable from quasi-static (aseismic) features because similar structures may hypothetically be formed by nonunique combinations of different variables (i.e., stress, deformation rate, temperature, etc.).

In a series of laboratory studies that provided the first experimental evidence of super-shear (greater than the shear wave velocity, c_s) crack growth in an isotropic and homogeneous solid (Homalite-100), Rosakis et al. (2000) observed and analyzed an array of secondary

tensile microcracks that formed adjacent to the rupture interface. These microcracks formed dynamically only on one side of the rupture interface (Rosakis et al., 2000). Their occurrence was attributed to dynamic frictional contact and sliding behind the supershear rupture tip (Rosakis et al., 2000; Samudrala et al., 2002). The possible relation of these cracks to geological observations of periodic arrays of tensile, off-fault, fractures and to pseudotachylyte injection veins was hypothesized by Rosakis (2002).

Di Toro et al. (2005a) provided field evidence that tensile fractures containing pseudotachylyte (pseudotachylyte injection veins) might indeed form by a similar dynamic process. Pseudotachylyte injection veins along exhumed strike-slip faults in the Adamello Batholith in the Italian Alps are observed in quasi-periodic arrays dominantly on one side of and nearly orthogonal to the faults. Such high-angle veins also are common along other pseudotachylyte-bearing faults (e.g., Swanson, 1988), and they differ from wing cracks commonly observed near tips of shear discontinuities (faults, sheared joints, and slipped bedding surfaces) related to the quasi-static perturbed stress field introduced by the shearing (Willemsse and Pollard, 1998; Mutlu and Pollard, 2008).

If pseudotachylyte injection veins are a dynamic phenomenon related to earthquake propagation, the geometry of tensile crack arrays should provide information about rupture dynamics from exhumed faults. To test this hypothesis, we designed an experiment capable of providing values of relevant variables during dynamic tensile microcrack nucleation accompanying high-speed shear rupture.

LABORATORY EXPERIMENTS

The experimental conditions under which tensile microcrack arrays were initially produced (Rosakis et al., 2000; Samudrala et al., 2002) utilized an impact-loading device to nucleate unilateral supershear ruptures. These experiments did not simulate earthquake rupture conditions expected along faults in that the interface was entirely free of compressive prestress. In addition, the nature of the impact loading introduced complex transients to the experiments, making correlations between crack angle, rupture velocity, and far-field static prestress conditions difficult. In a second set of experiments, sub-Rayleigh and supershear bilateral ruptures were produced in samples subjected to static uniaxial precompression (Xia et al., 2004, 2005; Lykotrakis et al., 2006; Lu et al., 2007). In these experiments, dynamic ruptures propagated along a frictional (but cohesionless) interface and were induced by an exploding wire embedded within the Homalite; however, tensile microcracks, like those observed along natural faults (Swanson, 1988; Di Toro et al., 2005a) and those predicted by numerical experiments (Yamashita, 2000; Di Toro et al., 2005a), were not produced in these experiments because transient stress concentrations associated with the propagating shear rupture tip did not exceed the material tensile strength.

Here, we report for the first time the generation of tensile microcracks that formed dynamically behind a sub-Rayleigh shear rupture propagating along a preexisting interface with cohesive and frictional strength, subjected to compressive and shear pre-tress (Fig. 1). Transient stress fields during the experiments were recorded using photoelasticity (Kavaturu et al., 1998) and high-speed digital photography (e.g., Rosakis, 2002), yielding patterns of isochromatic fringes (Fig. 2), which are contours of maximum in-plane shear stress. The asymmetric fringe pattern about the propagating rupture tip (Figs. 2A and 2B) is a result of a superposition of the static ambient stress, or pre-stress state (Poliakov et al., 2002; Samudrala et al., 2002), on the transient field around the propagating rupture. Written in indicial notation, the local stress state, σ_{ij} , in the vicinity of the propagating shear rupture tip can be written as:

$$\sigma_{ij} = \sigma_{ij}^0 + \sigma_{ij}^p \quad (1)$$

*Current address: Istituto Nazionale di Geofisica e Vulcanologia, Via di Vigna Murata 605, 00143 Rome, Italy; E-mail: griffith@ingv.it.

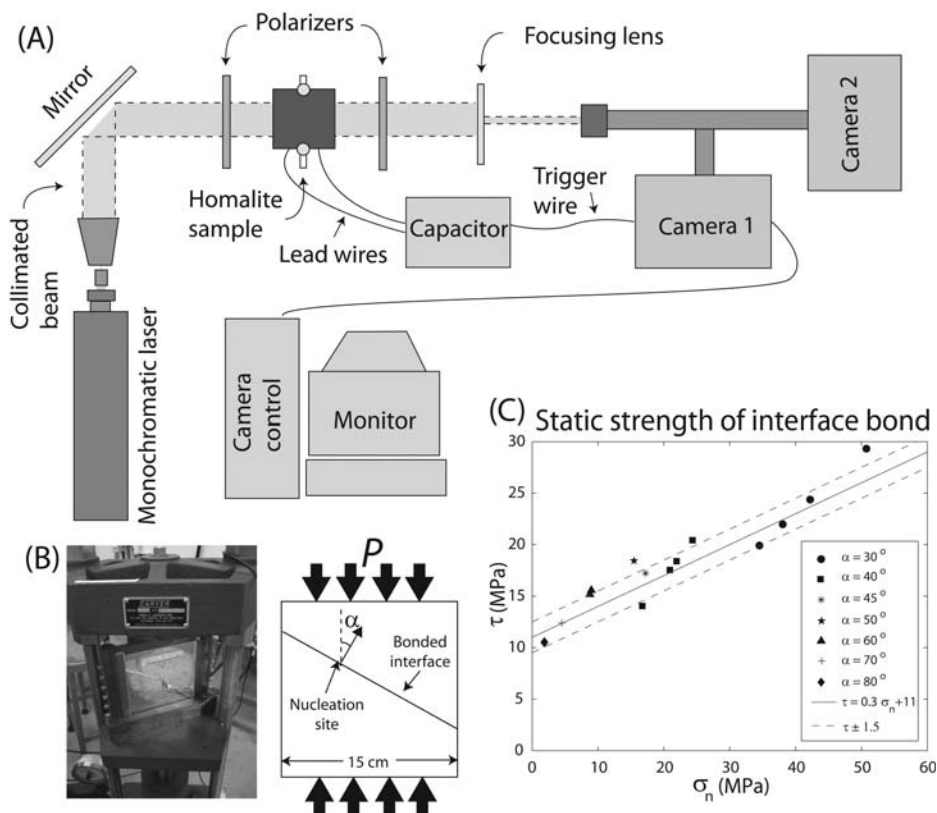
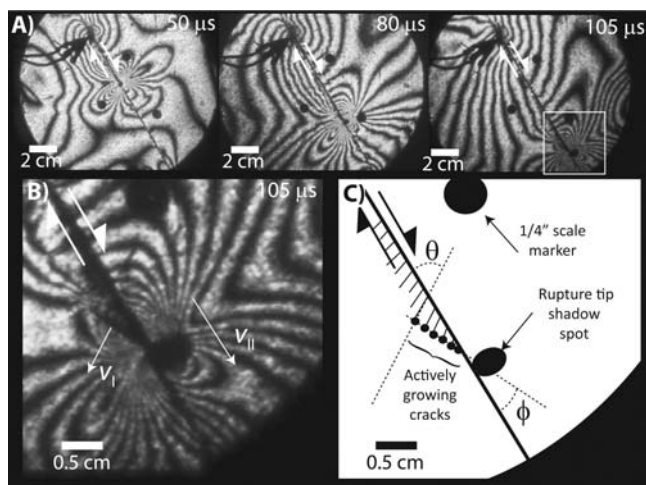


Figure 1. A: Photoelastic apparatus including laser light source, polarizing filters, and high-speed cameras. B: Hydraulic press and sample configuration showing relative orientation of vertical load (P) and inclination of interface (α). Explosion induces a bilateral right-lateral shear rupture upon explosion. C: To constrain parameters f_s (coefficient of static friction) and τ_o , we conducted static strength tests on 14 Homalite samples with glued interfaces at angles ranging from 30° to 80° using an Instron electromechanical testing machine. Samples were subjected to uniaxial loads in same configuration as shown in B. Experimental failure loads define a strength envelope with slope $f_s = 0.32 \pm 0.15$ and Y-intercept $\tau_o = 11.3 \pm 1.5$ MPa, where errors are plus or minus one standard deviation of residuals. See the GSA Data Repository (see footnote 1) for further detail.

Figure 2. Isochromatic fringe patterns around a shear rupture nucleating at an exploding wire and propagating along bonded interface. Note that fringes surrounding rupture tip expand as rupture grows, indicating an increasing stress concentration with distance. A: Photographs at 50, 80, and 105 μ s after detonation. White box in last photo indicates location of image in B. B: Close-up of rupture tip showing caustics associated with tensile microcrack tips. C: Schematic of B, identifying shadow spots, tensile microcracks, and defining angles θ and ϕ . All images are from experiment 601, with $P = 32$ MPa and $\alpha = 60^\circ$.



where σ_{ij}^0 is the static ambient stress state due to the remote load P , and $\Delta\sigma_{ij}$ is the stress perturbation due to the rupture (Poliakov et al., 2002).

Samudrala et al. (2002) and Poliakov et al. (2002) have shown that the off-fault stress concentration due to a propagating shear rupture is related to rupture velocity v_{II} and to peak shear traction τ_p attained along the rupture surface (i.e., shear stress needed to overcome total interface strength). In previous laboratory studies, this total interface strength τ_p was either due to cohesive strength, τ_o , of the glued bond (Samudrala et al., 2002), or to frictional strength, τ_f , of the interface due to the remote compressive stress P (Xia et al., 2004, 2005; Lu et al., 2007). Because cracks have not been observed to form in this frictional configuration, we applied an adhesive bond to the interface, thereby strengthening the interface by the amount τ_o (see the GSA Data Repository¹). The total interface strength is then:

$$\tau_p = \tau_f + \tau_o. \quad (2)$$

Here, τ_o is a constant material property of the bond, $\tau_f = f\sigma_n$, where f is the friction coefficient, and σ_n is normal traction resolved on the interface. Because transient stress state $\Delta\sigma_{ij}$ is proportional to total interface strength τ_p , adding cohesive strength τ_o should magnify off-fault stress, encouraging tensile failure of the Homalite. In the configuration shown in Figure 1B, the greatest tensile stress (and thus tensile cracking) is expected in the lower block for a rupture propagating downward to the right.

PRODUCTS OF DYNAMIC SHEAR RUPTURE

Ruptures in these experiments propagated with velocities in the range $0.7c_s < v_{II} < 0.85c_s$, where in Homalite $c_s = 1255$ m/s (Fig. DR1 in the Data Repository). Photoelastic images reveal that tensile microcracks initiate within the region of stress concentration directly behind the dynamic shear rupture tip. Figure 2A shows fringe patterns at three times around a propagating rupture in an experiment with axial load $P = 32$ MPa and inclination angle $\alpha = 60^\circ$. A closer view of the shear rupture tip at 105 μ s (Fig. 2B) reveals a trailing line of dark spots at an acute angle to the interface. These are shadow spots surrounded by caustics (Rosakis et al., 2000) associated with propagating tensile microcrack tips (Fig. 2C). The trailing edge of this triangular zone marks the point at which the microcracks stop growing: behind this zone static microcracks are left in the wake of the propa-

¹GSA Data Repository item 2009195, summary of experimental methods and results, is available online at www.geosociety.org/pubs/ft2009.htm, or on request from editing@geosociety.org or Documents Secretary, GSA, P.O. Box 9140, Boulder, CO 80301, USA.

gating rupture (Figs. 2B and 2C; Video DR1 in the Data Repository). This zone, between 5 and 10 mm in length (Figs. 2B and 2C), corresponds to the shear cohesive (process) zone of the propagating shear rupture. These observations confirm that the microcrack formation is a dynamic phenomenon triggered by the transient stress field of a propagating shear rupture and that the microcracks grow only in close proximity to the shear rupture tip.

Tensile microcracks (Fig. 3) were produced during shear rupture in all experiments at $\alpha = 60^\circ$ and 70° , but microcracks were not observed at $\alpha = 80^\circ$. For greater values of α , remote compressive stress P resolves lesser normal and shear tractions on, and greater compression parallel to, the interface, which would inhibit tensile cracking. Consistent with theoretical calculations (Samudrala et al., 2002), all cracks formed in the tensile quadrant, nucleated on the interface, and grew into the Homalite (Fig. 3). In all cases, microcracks formed at high angles to the rupture interface and some curved slightly as they propagated into the Homalite sample (Fig. 3B). Longer microcracks typically were interspersed with shorter microcracks, and crack size and spacing were greater at $\alpha = 60^\circ$ than $\alpha = 70^\circ$. Maximum microcrack length changed systematically with distance from the nucleation site of the shear rupture, increasing from initial occurrence at ~ 3 cm to a maximum (as much as ~ 5 mm in length at $\alpha = 60^\circ$) at ~ 9 cm, and then the length steadily decreased toward the edge of the sample (e.g., Fig. 3A). The increase in microcrack dimension with distance from the nucleation site was accompanied by an increase in stress concentration as evidenced by expansion of the lobes in the fringe pattern focused around the rupture tip (Fig. 2A). Microcracks typically were shorter for greater rupture interface inclination angles α , reaching a maximum length of ~ 2.5 cm at $\alpha = 70^\circ$. Longer microcracks extended across the entire thickness of the sample, while shorter microcracks did not (Fig. 3C). For $\alpha = 60^\circ$, the average width (measured across the out-of-plane dimension of the specimen) of microcracks was 0.35 ± 0.16 cm, whereas the average width for $\alpha = 70^\circ$ was 0.25 ± 0.19 cm. Average microcrack spacing for $\alpha = 60^\circ$ was 0.35 ± 0.29 cm, whereas spacing for $\alpha = 70^\circ$ was 0.23 ± 0.13 cm. The larger microcrack width at a smaller inclination angle is consistent with overall larger relative crack size as suggested by the length measurements. Average crack spacing appears to have a weak, inverse dependence on v_{II} , tending to be smaller at faster v_{II} .

Tensile microcracks grew in the velocity range $0.25c_s < v_1 < 0.33c_s$ (Fig. DR2). The microcracks were never observed to branch, which is consistent with propagation velocities on the order of $v_1 \approx 0.3c_s$, less than the critical

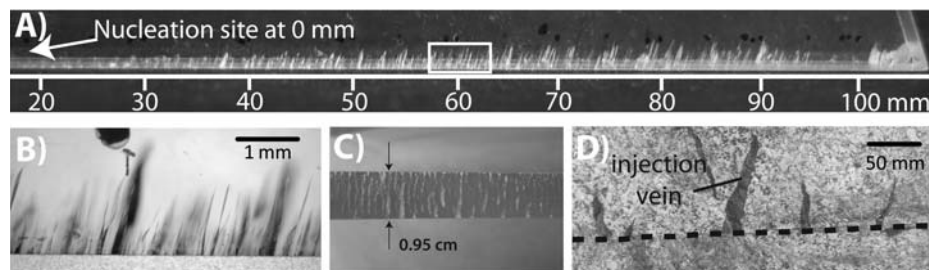


Figure 3. Tensile microcracks in Homalite 100 specimen 70I, $P = 38$ MPa and $\alpha = 60^\circ$. A: View of 10-cm-long array of microcracks along rupture interface. White box shows location of image shown in B. B: Transmitted light microscopic image of microcracks. C: View of rupture interface surface. Larger microcracks frequently extend across sample thickness, while smaller microcracks only partially cut sample. Samples are ~ 0.95 cm in thickness. D: Photograph of pseudotachylyte injection veins along a fault in Adamello Batholith.

branching velocity (e.g., Fineberg et al., 1991; Sagy et al., 2001, 2002).

The inclination angle θ (Fig. 3C; Fig. DR1) between tensile microcrack and interface for cracks longer than ~ 0.1 mm was measured on photomicrographs taken with an optical microscope focused at midthickness of the Homalite samples. Microcrack orientation, θ , varied within individual experiments by as much as $\sim 15^\circ$ (Fig. DR1). By comparing θ and v_{II} variations from all experiments, it is clear that θ correlates with v_{II} ; however, v_{II} is not the only parameter that influences microcrack inclination.

To compare experiments, we binned microcrack orientation data from velocity-distance plots (e.g., Fig. DR1) using bin centers at locations where rupture velocities were calculated. In Figure 4, we plot average crack angle θ over each bin against the corresponding rupture velocity for each experiment. These data are from six experiments representing two different loading configurations ($\alpha = 70^\circ$, $P = 38$ MPa; and $\alpha = 60^\circ$, $P = 32$ MPa). Two distinct trends show inclination angle increasing almost lin-

early with rupture velocity. The offset between the two trends is a measure of the influence of σ_{ij}^0 on microcrack orientation, i.e., $\Delta\theta = 7^\circ\text{--}8^\circ$ for $\Delta P = 6$ MPa and $\Delta\alpha = 10^\circ$.

DISCUSSION AND CONCLUSIONS

These experiments yielded a series of important insights into tensile cracking around a propagating subsonic shear rupture subjected to compressive and shear prestress. Most importantly, we established that the tensile microcracks are a dynamic phenomenon not confined to experiments performed under impact loading in the absence of static compressive stress. The opening microcracks formed systematically in the region of tensile stress concentration on one side of the propagating shear rupture, consistent with early experimental results (Rosakis et al., 2000), field interpretations (Di Toro et al., 2005a), and theoretical predictions (Samudrala et al., 2002; Di Toro et al., 2005a). This phenomenon was not observed in laboratory experiments using a similar configuration with identical materials but absent interfacial cohesion (e.g., Lu et al.,

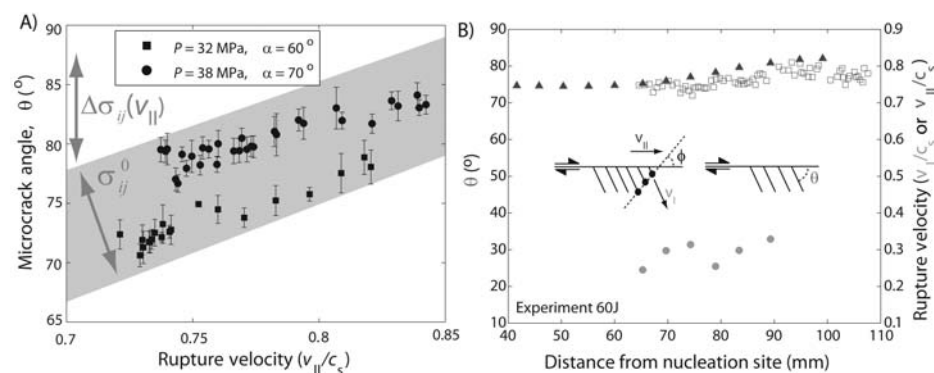


Figure 4. A: Summary plot of average θ versus shear rupture velocities for six experiments. Inclination of data trends represents dependence of microcrack orientation on transient stress $\Delta\sigma_{ij}$, which is dependent on rupture velocity v_{II} . Offset between two trends is a function of background, prestress state, σ_{ij}^0 . Error bars represent \pm one standard deviation for each interval plotted. B: Example of rupture velocity and crack angle data from experiment 60J. Empty squares are microcrack inclination angle (θ) measurements, filled triangles are average v_{II} , and filled circles are average v_I .

2007). The necessity of cohesion speaks to the competing effect of frictional strength and fracture toughness in enabling or retarding formation of microcracks: fault damage in the form of tensile fracture should be more prevalent along “strong” faults (e.g., stress drop > 100 MPa, as defined by Kanamori [1994]), even in the presence of large compressive tectonic stress. Finally, the direction of tensile microcrack growth always makes an acute angle with the direction of shear rupture growth (Fig. 2).

Several other observations are thought-provoking and require further investigation. First, microcrack growth initiates on the interface near the shear rupture tip, and growth ceases when the rupture tip has moved ~5–10 mm beyond the microcrack. The orientation at which microcracks initiate is related to rupture velocity, v_{II} , and tectonic stress state (Fig. 4). We can quantify these effects using an analytical solution for a dynamic mode II crack following Samudrala et al. (2002). Such an analysis requires knowledge of the velocity weakening behavior and the ultimate tensile strength of the monolithic Homalite material, parameters that are difficult to determine independently. Using measurements of rupture velocity, crack angle, and static prestress state, we can inversely constrain these elusive parameters that are critical to defining the physics at the rupture tip. These insights will be detailed in subsequent work.

Ruptures consistently propagate between 0.7 and $0.85c_s$. Theoretically, however, a mode II crack propagating along a weak path in a homogeneous, isotropic elastic material should approach the Rayleigh wave speed ($c_R = 0.92c_s$). High stresses associated with rupture velocities approaching c_s can lead to energy dissipation due to inelastic yielding (e.g., Andrews, 2005; Yamashita, 2000) around the crack tip, lowering the terminal rupture velocity. Such an effect has been measured directly in the laboratory for mode I (opening) fractures (Sharon et al., 1996). The formation of damage in the present study (i.e., creation of new fracture surface area) certainly created an energy sink, lowering terminal rupture velocity. An important question to pursue in future work is: Does creation of new surfaces account for the energy deficit responsible for sub-Rayleigh rupture propagation?

This study suggests a fundamental connection between tensile, off-fault fractures and past earthquakes since the laboratory tensile microcracks are shown to be produced dynamically by transient stress perturbations due to a rapidly propagating shear rupture. Furthermore, we demonstrate that microcrack orientations correlate with rupture velocity and ambient stress. Beyond simply elucidating

such relationships, this study provides avenues for advancing understanding of them: because we have been able to visualize the phenomenon dynamically and identify the relevant parameters, we can now take steps to construct and verify analytical models to investigate the interplay among fault damage, rupture velocity, and tectonic conditions.

ACKNOWLEDGMENTS

Griffith and Pollard were supported by the U.S. Geological Survey (USGS), Department of Interior, under USGS award number 08HQGR0010. Griffith also received support under National Science Foundation (NSF) grant OISE-0754258. Rosakis and Ko were supported by U.S. Department of Energy grant DE-FG52-06NA 26209, NSF grant EAR-0711545, and Office of Naval Research Multidisciplinary Research Initiative (ONR MURI) grant N0014-06-1-0730.

REFERENCES CITED

- Andrews, D. J., 2005, Rupture dynamics with energy loss outside the slip zone: *Journal of Geophysical Research*, v. 110, doi: 10.1029/2004JB003191.
- Chester, F.M., Evans, J.P., and Biegel, R.L., 1993, Internal structure and weakening mechanisms of the San Andreas fault: *Journal of Geophysical Research*, v. 98, p. 771–786, doi: 10.1029/92JB01866.
- Cowan, D., 1999, Do faults preserve a record of seismic slip?—A field geologist’s opinion: *Journal of Structural Geology*, v. 21, p. 2703–2719, doi: 10.1016/S0191-8141(99)00046-2.
- Di Toro, G., Nielsen, S., and Pennacchioni, G., 2005a, Earthquake rupture dynamics frozen in exhumed ancient faults: *Nature*, v. 436, p. 1009–1012, doi: 10.1038/nature03910.
- Di Toro, G., Pennacchioni, G., and Teza, G., 2005b, Can pseudotachylites be used to infer earthquake source parameters? An example of limitations in the study of exhumed faults: *Tectonophysics*, v. 402, p. 3–20, doi: 10.1016/j.tecto.2004.10.014.
- Fineberg, J., Gross, S.P., Marder, M., and Swinney, H.L., 1991, Instability in dynamic fracture: *Physical Review Letters*, v. 67, p. 457–460, doi: 10.1103/PhysRevLett.67.457.
- Griffith, W.A., Di Toro, G., Pennacchioni, G., and Pollard, D.D., 2008, Thin pseudotachylites in faults of the Mt. Abbot Quadrangle, Sierra Nevada California: Physical constraints on seismic slip: *Journal of Structural Geology*, v. 30, p. 1086–1094, doi: 10.1016/j.jsg.2008.05.003.
- Kanamori, H., 1994, Mechanics of earthquakes: *Annual Review of Earth and Planetary Sciences*, v. 22, p. 207–237.
- Kavaturu, M., Shukla, A., and Rosakis, A.J., 1998, Intersonic crack propagation along interfaces: Experimental observations and analysis: *Journal of Experimental Mechanics*, v. 38, p. 218–225, doi: 10.1007/BF02325746.
- Lu, X., Lapusta, N., and Rosakis, A.J., 2007, Pulse-like and crack-like ruptures in experiments mimicking crustal earthquakes: *Proceedings of the National Academy of Sciences of the United States of America*, v. 104, p. 18,931–18,936, doi: 10.1073/pnas.0704268104.
- Lykotraftis, G., Rosakis, A.J., and Ravichandran, G., 2006, Self-healing pulse-like shear ruptures in

the laboratory: *Science*, v. 313, p. 1765–1768, doi: 10.1126/science.1128359.

- Mutlu, O., and Pollard, D.D., 2008, On the patterns of wing cracks along an outcrop scale flaw: A numerical modeling approach using complementarity: *Journal of Geophysical Research*, v. 113, doi: 10.1029/2007JB005284.
- Poliakov, A.N.B., Dmowska, R., and Rice, J.R., 2002, Dynamic shear rupture interactions with fault bends and off-axis secondary faulting: *Journal of Geophysical Research*, v. 107, doi: 10.1029/2001JB000572.
- Rosakis, A.J., 2002, Intersonic shear cracks and fault ruptures: *Advances in Physics*, v. 51, p. 1189–1257, doi: 10.1080/00018730210122328.
- Rosakis, A.J., Samudrala, S., and Coker, D., 2000, Intersonic shear crack growth along weak planes: *Materials Research Innovation*, v. 3, p. 236–243, doi: 10.1007/s100190050009.
- Sagy, A., Reches, Z., and Roman, I., 2001, Dynamic fracturing: Field and experimental observations: *Journal of Structural Geology*, v. 23, p. 1223–1239, doi: 10.1016/S0191-8141(00)00190-5.
- Sagy, A., Reches, Z., and Fineberg, J., 2002, Dynamic fracture by large extraterrestrial impacts as the origin of shatter cones: *Nature*, v. 418, p. 310–313, doi: 10.1038/nature00903.
- Samudrala, O., Huang, Y., and Rosakis, A.J., 2002, Subsonic and intersonic shear rupture of weak planes with a velocity weakening cohesive zone: *Journal of Geophysical Research*, v. 107, doi: 10.1029/2001JB000460.
- Sharon, E., Gross, S.P., and Fineberg, J., 1996, Energy dissipation in dynamic fracture: *Physical Review Letters*, v. 76, p. 2117–2120.
- Swanson, M.T., 1988, Pseudotachylite-bearing strike-slip duplex structures in the Fort Foster brittle zone, S. Maine: *Journal of Structural Geology*, v. 10, p. 813–828, doi: 10.1016/0191-8141(88)90097-1.
- Wibberley, C.A.J., and Shimamoto, T., 2003, Internal structure and weakening effects of major strike-slip fault zones: The Median Tectonic Line in Mie Prefecture, southwest Japan: *Journal of Structural Geology*, v. 25, p. 59–78, doi: 10.1016/S0191-8141(02)00014-7.
- Willemse, E.J.M., and Pollard, D.D., 1998, On the orientation and patterns of wing cracks and solution surfaces at the tips of a sliding flaw or fault: *Journal of Geophysical Research*, v. 103, p. 2427–2438, doi: 10.1029/97JB01587.
- Xia, K., Rosakis, A.J., and Kanamori, H., 2004, Laboratory earthquakes: The sub-Rayleigh-to-supershear rupture transition: *Science*, v. 303, p. 1859–1861, doi: 10.1126/science.1094022.
- Xia, K., Rosakis, A.J., Kanamori, H., and Rice, J.R., 2005, Laboratory earthquakes along inhomogeneous faults: Directionality and supershear: *Science*, v. 308, p. 681–684.
- Yamashita, T., 2000, Generation of microcracks by dynamic shear rupture and its effects on rupture growth and elastic wave radiation: *Geophysical Journal International*, v. 143, p. 395–406, doi: 10.1046/j.1365-246X.2000.01238.x.

Manuscript received 23 January 2009

Revised manuscript received 15 April 2009

Manuscript accepted 26 April 2009

Printed in USA